Theoretical Investigation of Molecular Properties of the First Excited State of the Thiophenoxyl Radical

Chi-Wen Cheng, Yuan-Pern Lee, and Henryk A. Witek*

Institute of Molecular Science and Department of Applied Chemistry, National Chiao Tung University, 30010 Hsinchu, Taiwan

Received: June 9, 2008; Revised Manuscript Received: September 29, 2008

Accurate ab initio study of the lowest excited state (A $^2B_2$) of the thiophenoxyl radical is presented. The calculated equilibrium geometries, excitation energies, and harmonic vibrational frequencies show that the A $^2B_2 \leftarrow$ X $^2B_1$ excitation in C_6H_5S has different characteristics than the analogous transition in the phenoxyl radical. Vertical excitation energies for other low-lying (<4.5 eV) excited states of the thiophenoxyl radical are also presented and compared with available experimental data.

Introduction

Sulfur-containing radicals attracted considerably less attention than their oxygen analogues. Accordingly, the structure and spectroscopy of the thiophenoxyl radical (C_6H_5S, aka the phenylthiyl, phenylsulfyl, or phenylsulfur radical) is far less studied than the corresponding properties of the phenoxyl radical.

A number of absorption bands were reported in solution,[1−11] solid matrix,[12−14] and gas-phase[15−17] experiments. No definitive assignment of the observed peaks to particular electronic states of C_6H_5S was given. Most of the experimental effort was devoted to kinetics and possible reaction pathways of the C_6H_5S radical, which was produced via flash photolysis,[2−6] laser flash photolysis,[1,7] or pulse radiolysis[8,9,11] of liquid or solvated aromatic sulfur compounds. The main spectral tool to monitor this radical was the broad transient UV−vis absorption near 297 and 490 nm. It is noteworthy that the vibrational structure of these bands is not well-defined. Upon photolysis of solid samples of thiophenol or diphenyl disulfide, two bands appeared in the emission spectra. These experiments were performed in 3MP (3-methylpentane) or EPA (a mixture of ethyl ether, isopentane, and ethanol) matrices at 77K. The first band[12−14] was observed in the region 626−770 nm (red emission, 1.61−1.98 eV) and had a long lifetime. The second band[13,14] had a short lifetime with maximal intensity at 435 nm (broad intense blue emission, 2.85 eV).

Two transient absorption bands were attributed to gaseous C_6H_5S, one around 310 nm[15,18] and the other around 470−520 nm.[16] The laser-induced fluorescence excitation spectrum[17] of gaseous C_6H_5S in the region 490−520 nm exhibited a transition origin at 517.38 nm (2.396 eV). The transition origin was tentatively assigned to the $^2A_2 \leftarrow {}^2B_2$ excitation. (Note that this assignment is erroneous; the lower state should be $^2B_1$.) Three vibrational frequencies (275, 410, and 483 cm^{-1}) were determined for the $^2A_2$ electronic state. A recent dynamic investigation[19−21] of photodissociation of thiophenol revealed that the lowest excited state (A $^2B_2$) of C_6H_5S might be located at 2580 cm^{-1} (0.32 eV).

Six fully symmetric vibrational frequencies (436, 724, 991, 1073, 1180, and 1551 cm^{-1}) for the ground electronic state of C_6H_5S in solution were reported by Tripathi et al. based on their resonance Raman experiment. This study indicated that the CS bond in C_6H_5S has essentially a single character with the unpaired electron localized on the sulfur atom.[10] Three vibrational frequencies (430, 610, and 1165 cm^{-1}) were determined for the ground electronic state from observed progressions in the dispersed fluorescence spectrum of gaseous C_6H_5S.[17] No experimental information on the equilibrium structure of C_6H_5S is available.

Theoretical calculations of equilibrium geometry and harmonic vibrational frequencies were reported for the ground (X $^2B_1$) state[10,22−25] and the first excited (A $^2B_2$) state.[24] No reliable quantum chemical predictions are available for higher electronic states of C_6H_5S.

In a recent study[26] we presented an analysis of molecular properties of the phenoxyl radical (C_6H_5O) in its first excited state, A $^2B_2$. A comparison of calculated equilibrium geometries and vibrational frequencies between the ground and excited states showed relatively large structural changes upon the A $^2B_2 \leftarrow$ X $^2B_1$ transition. The A $^2B_2 \leftarrow$ X $^2B_1$ excitation energy[27,28] for C_6H_5O (1.1 eV) is significantly larger than the corresponding experimental value reported recently for C_6H_5S (0.32 eV).[19−21] It is of fundamental interest[29] to understand how the replacement of oxygen by sulfur alters the energetics, structure, and vibrational spectra upon analogous excitation. A detailed theoretical analysis of various molecular properties of the lowest excited *A* $^2B_2$ state of C_6H_5S, together with a comparison with C_6H_5O, is presented in this study. The main motivation for our study is a perspective of accurate experimental characterization of the optically forbidden A $^2B_2 \leftarrow$ X $^2B_1$ transition of C_6H_5S using the cavity ringdown absorption technique, which requires detailed information on energetics and vibrational frequencies of the A $^2B_2$ state.

Computational Details

Most of computational details are identical to those in the previous study of the phenoxyl radical.[25] The molecular model of the thiophenoxyl radical is shown in Figure 1. The symmetry of the ground state is described as a doublet B_1 and the symmetry of the first excited state as a doublet B_2. The presented energetics and equilibrium geometries have been calculated using complete active space second-order perturbation theory[30,31] (CASPT2) and density functional theory (DFT). In addition, the cluster-corrected (Davidson correction) multireference configuration interaction (MRCI+Q) vertical and adiabatic excita-

* Corresponding author. E-mail: hwitek@mail.nctu.edu.tw.

10.1021/jp805045s CCC: $40.75
Published on Web 10/24/2008

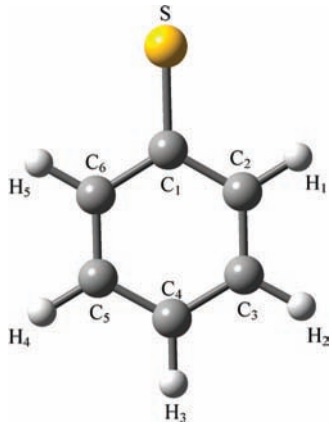

Figure 1. Molecular structure (C_{2v}) of the thiophenoxyl radical in the $X\ ^2B_1$ and $A\ ^2B_2$ electronic states.

tion energetics for the $A\ ^2B_2$ state has been computed at the optimized CASPT2 geometries in the space of single and double excited configurations using the CASSCF wave function as a reference. Analogous MRCI+Q results for the phenoxyl radical are obtained in a similar way. Vertical excitation energies of low-lying excited states of the thiophenoxyl radical have been computed using the TDDFT[32] (time-dependent DFT) and multistate (MS) CASPT2[33] formalisms. For computing the harmonic frequencies, DFT has been employed. The presented results are obtained with a series of four basis sets: cc-pVDZ, aug-cc-pVDZ, cc-pVTZ, and aug-cc-pVTZ.[34,35] For the CASSCF, CASPT2, and MRCI calculations, we have used the MOLPRO program.[36] The DFT and TDDFT calculations have been carried out with the Gaussian package[37] using the B3LYP functional[38,39] together with the unrestricted Kohn−Sham formalism.[40] The complete active space (CAS) in the CASSCF, CASPT2, and MRCI calculations is constructed using all valence π orbitals (two of symmetry a_2 and five of symmetry b_1) and one σ orbital of symmetry b_2 corresponding to the lone pair on the sulfur atom. The resulting active space, ($0a_1$, $2a_2$, $5b_1$, $1b_2$), correlates nine active electrons. In the calculation of CASPT2 vertical excitation energies for higher excited states, this CAS space has been augmented with an additional occupied σ orbital of symmetry a_1 (the other lone pair on sulfur) to allow for proper description of the $^2A_1$ state. In the MRCI and CASPT2 calculations, the [He] inner shell of carbon and the [Ne] inner shell of sulfur have not been correlated.

Results

a. Geometrical and Electronic Structure of the A $^2B_2$ State. Optimized geometrical parameters (see Figure 1) for the ground and first excited state of the thiophenoxyl radical are given in Table 1. The equilibrium bond distances and angles have been calculated using the CASPT2 and DFT approaches. The systematic sequence of four basis sets used in our calculations shows that the computed bond distances depend on the quality of the basis set, giving bond shortening of approximately 0.01 Å upon substituting cc-pVDZ with cc-pVTZ. It is possible that bond distances computed in the complete basis set limit would be even shorter. The quality of the basis set does not affect the equilibrium angles. Augmenting the basis sets with diffuse functions has no effect on equilibrium structures. The difference between the geometrical parameters from DFT and CASPT2 is negligible for the CH bonds and angles, while for r_{CC} and r_{CS}, the difference can be as large as 0.012 Å. This discussion allows for estimating the accuracy of the calculated structural parameters as ±0.01 Å for bond distances and ±0.2° for equilibrium angles. The most plausible estimates (in Å) of bond distances in C_6H_5S are given thus as averaged values of the DFT and CASPT2 parameters at the aug-cc-pVTZ level: $r_{C_1S} = 1.717$, $r_{C_1C_2} = 1.416$, $r_{C_2C_3} = 1.385$, $r_{C_3C_4} = 1.398$, and $r_{CH} = 1.081$ for the $X\ ^2B_1$ state and $r_{C_1S} = 1.758$, $r_{C_1C_2} = 1.400$, $r_{C_2C_3} = 1.392$, $r_{C_3C_4} = 1.392$, and $r_{CH} = 1.081$ for the $A\ ^2B_2$ state. These values are used in the following discussion. The structural parameters reported here should be superior to the previously published theoretical data in terms of the quality of the employed basis set.[10,22−25] Note that this is especially important for proper description of the structure of the benzene ring in the thiophenoxyl radical, since calculations in smaller basis sets[21,24] seem to overestimate the quinoid character of the ground state structure.

In benzene, the experimental length of the CC bond is 1.397 Å.[41] In *p*-benzoquinone, the regular benzene pattern is alternated with $r_{C_1C_2} = r_{C_3C_4} = 1.477$ Å and $r_{C_2C_3} = 1.322$ Å.[42] A comparison with the calculated r_{CC} values shows that the structure of the benzene ring in C_6H_5S in both electronic states is aromatic with only little quinoid character for the $X\ ^2B_1$ state. This situation is in contrast to that reported for the ground state structure of the phenoxyl radical ($r_{C_1C_2} = 1.448$ Å, $r_{C_2C_3} = 1.375$ Å, and $r_{C_3C_4} = 1.406$ Å), which could be described as intermediate between aromatic and quinoid.[26,43] Similar contrast can be observed for the separation between the heteroatom and the benzene ring. The calculated length of the CS bond in both electronic states is intermediate between single and double bond. Compare the calculated values of 1.717 ($X\ ^2B_1$) and 1.758 Å ($A\ ^2B_2$) with typical lengths of single (1.835 Å in thietane, 1.835 Å in tetrahydrothiophene, 1.818 Å in methanethiol, 1.791 Å in the thiomethoxyl radical, 1.77 Å in thiophenol, and 1.714 Å in thiophene)[41,44] and double CS bonds (1.681 Å in thioureas, 1.611 Å in thioformaldehyde, 1.610 Å in thioacetaldehyde, and 1.554 Å in carbon disulfide).[41,45] The difference between the CS bond lengths in both studied states of the thiophenoxyl radical ($\Delta r_{CS} = 0.04$ Å) is noticeably smaller than the analogous value for the phenoxyl radical ($\Delta r_{CO} = 0.07$ Å). It is interesting to note that r_{CS} for the $X\ ^2B_1$ state of C_6H_5S is almost identical to this in thiophene, while for $X\ ^2B_1$ of C_6H_5O, the r_{CO} distance (1.254 Å)[26] is noticeably shorter than this in furan (1.362 Å).[41] It is clear from this discussion that the molecular structures of the ground states of the phenoxyl and thiophenoxyl radicals are rather distinct, while for the first excited state of both radicals, close structural similarity can be observed. We use this observation in the next two sections to interpret the different spectroscopy of both radicals.

Close analogy can be observed for the electronic structure of both radicals. Similar to the situation for C_6H_5O, the wave function of both studied states of C_6H_5S can be adequately described using a single Slater determinant: $|\sigma_{b_2}^2\pi_{b_1}^2\sigma_{a_1}^2\pi_{b_1}^2\pi_{a_2}^2\pi_{b_1}^0\pi_{a_2}^{*0}\pi_{b_1}^{*0}\pi_{b_1}^{*0}\rangle$ for the $X\ ^2B_1$ state and $|\pi_{b_1}^2\sigma_{a_1}^2\pi_{b_1}^2\pi_{a_2}^2\pi_{b_1}^2\sigma_{b_2}^1\pi_{a_2}^{*0}\pi_{b_1}^{*0}\pi_{b_1}^{*0}\rangle$ for the $A\ ^2B_2$ state. The weight of these Slater determinants in the multiconfigurational CASSCF wave functions is 86% and 89%, respectively. After including dynamic correlation, these values diminish to 63% and 65%, respectively (aug-cc-pVTZ). The weight of other determinants, mostly corresponding to various distributions of π electrons in the π orbitals of the benzene ring, is small (<2% at the CASSCF level). The main chemical difference between the ground states of C_6H_5O and C_6H_5S comes thus from the variation of the orbital set used for constructing the wave functions. A schematic energy pattern for the active orbitals for both states of C_6H_5S is shown in Figure 2. This scheme is almost identical to that presented

TABLE 1: Geometrical Parameters for the X $^2B_1$ and A $^2B_2$ States of the Thiophenoxyl Radical Optimized Using CASPT2 and B3LYP[a]

	cc-pVDZ		aug-cc-pVDZ		cc-pVTZ		aug-cc-pVTZ	
	CASPT2	B3LYP	CASPT2	B3LYP	CASPT2	B3LYP	CASPT2	B3LYP
				X $^2B_1$				
r_{C_1S}	1.727	1.733	1.727	1.734	1.712	1.724	1.711	1.723
$r_{C_1C_2}$	1.430	1.422	1.432	1.422	1.418	1.414	1.419	1.414
$r_{C_2C_3}$	1.401	1.390	1.402	1.391	1.388	1.382	1.388	1.382
$r_{C_3C_4}$	1.412	1.403	1.414	1.403	1.400	1.395	1.401	1.395
$r_{C_2H_1}$	1.094	1.091	1.093	1.089	1.080	1.081	1.081	1.081
$r_{C_3H_2}$	1.094	1.092	1.093	1.090	1.080	1.082	1.081	1.082
$r_{C_4H_3}$	1.094	1.092	1.093	1.091	1.081	1.082	1.081	1.082
$\alpha_{C_6C_1C_2}$	118.5	118.4	118.7	118.5	118.6	118.4	118.7	118.4
$\alpha_{C_1C_2C_3}$	120.6	120.6	120.4	120.5	120.5	120.6	120.4	120.6
$\alpha_{C_2C_3C_4}$	120.1	120.1	120.1	120.1	120.1	120.1	120.1	120.1
$\alpha_{C_1C_2H_1}$	118.5	118.4	118.4	118.6	118.4	118.5	118.4	118.6
$\alpha_{C_4C_3H_2}$	120.0	120.0	120.0	120.0	120.0	120.0	119.9	120.0
				A $^2B_2$				
r_{C_1S}	1.769	1.774	1.771	1.774	1.753	1.763	1.753	1.763
$r_{C_1C_2}$	1.414	1.406	1.415	1.406	1.402	1.398	1.402	1.398
$r_{C_2C_3}$	1.406	1.397	1.408	1.397	1.394	1.389	1.394	1.389
$r_{C_3C_4}$	1.407	1.398	1.409	1.398	1.395	1.390	1.395	1.390
$r_{C_2H_1}$	1.094	1.092	1.093	1.092	1.081	1.081	1.082	1.081
$r_{C_3H_2}$	1.095	1.093	1.093	1.093	1.081	1.082	1.081	1.082
$r_{C_4H_3}$	1.094	1.092	1.093	1.092	1.080	1.081	1.081	1.081
$\alpha_{C_6C_1C_2}$	119.7	119.6	119.9	119.6	119.9	119.6	119.9	119.6
$\alpha_{C_1C_2C_3}$	119.8	119.8	119.7	119.8	119.7	119.8	119.7	119.8
$\alpha_{C_2C_3C_4}$	120.6	120.7	120.7	120.7	120.6	120.7	120.6	120.7
$\alpha_{C_1C_2H_1}$	120.1	120.2	120.2	120.1	120.1	120.2	120.1	120.2
$\alpha_{C_4C_3H_2}$	120.2	120.2	120.1	120.2	120.2	120.1	120.1	120.1

[a] All CASPT2 calculations use the same ($0a_1$, $2a_2$, $5b_1$, $1b_2$) active space described in detail in the text. Distances are given in Å and bonds in deg. For an explanation of geometrical parameters, see Figure 1.

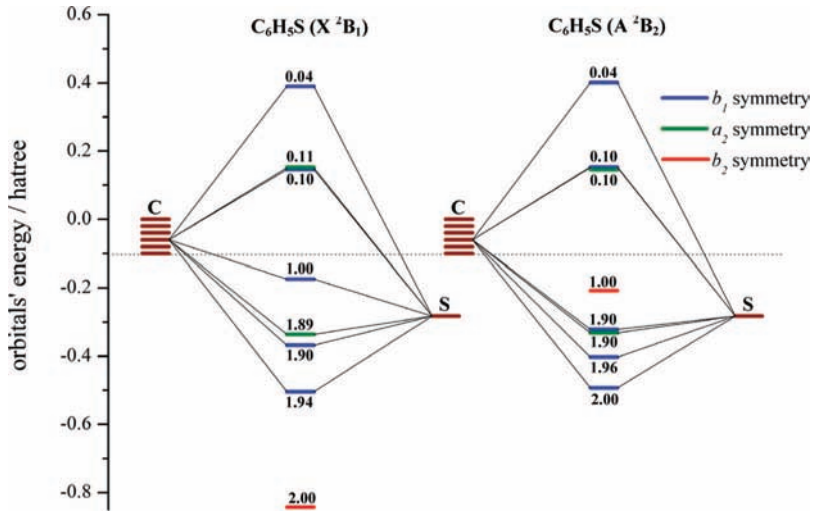

Figure 2. Orbital energy diagram for the seven active π orbitals and one active σ orbital of C_6H_5S in the X $^2B_1$ and A $^2B_2$ states obtained from the CASSCF($0a_1$, $2a_2$, $5b_1$, $1b_2$)/aug-cc-pVDZ calculations. Occupation numbers are given for every orbital.

earlier for the phenoxyl radical.[26] The only important difference concerns the chemical character of the singly occupied b_1 orbital (SOMO), which is almost completely localized on sulfur in C_6H_5S and strongly delocalized over oxygen and the aromatic ring in C_6H_5O. (See also the discussion in refs 9 and 10.) For C_6H_5S, the delocalization is hindered—as can be seen from the atomic spin densities shown in Figure 3—owing to a much larger distance between sulfur and the aromatic ring. This larger distance, originating from the larger size of the sulfur atom, does not permit effective overlap of the atomic p orbitals constituting the π manifold and consequently separates the π electron densities of the ring and sulfur. In C_6H_5O, where the distance is approximately 0.5 Å shorter, the coupling of the p orbitals is much larger. (Note that conventional chemical explanation in terms of the large difference between the atomic orbital energies does not apply here. The one-electron energy of the carbon 2p orbital is −0.467 hartree. For the sulfur 3p orbital, one has −0.428 hartree and for oxygen 2p orbital −0.616 hartree.[46]) Strong localization of the unpaired electron on sulfur for the X $^2B_1$ state of the thiophenoxyl radical can also be inferred from the experimental ESR and resonance Raman

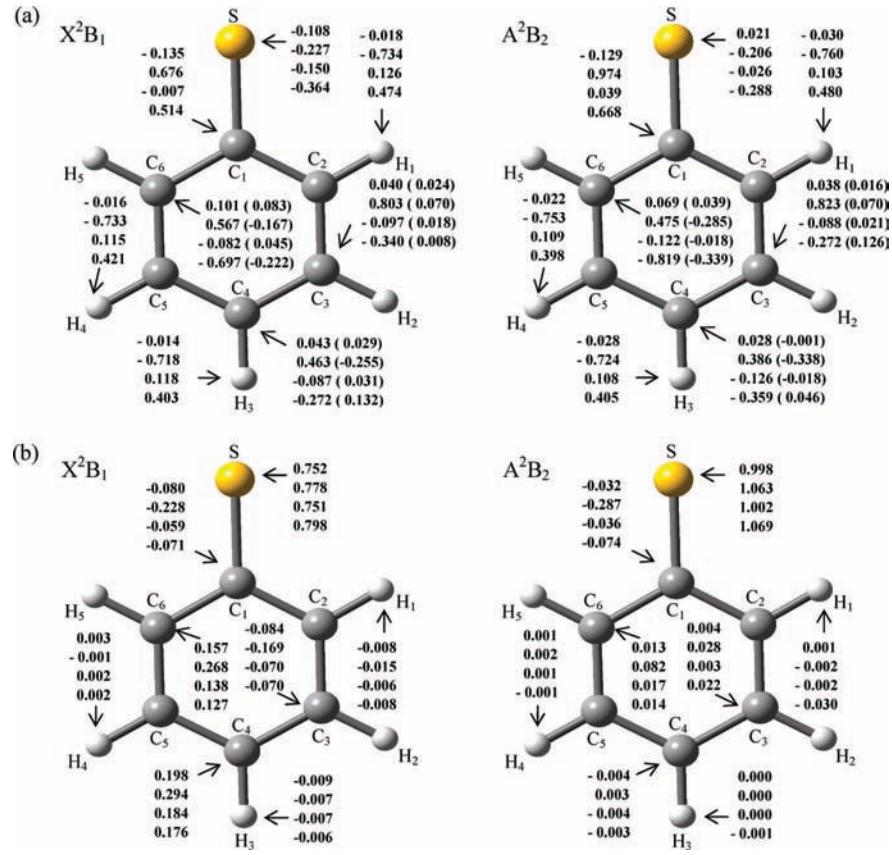

Figure 3. Mulliken charges (a) and spin densities (b) for the X $^2B_1$ and A $^2B_2$ states of C_6H_5S obtained from DFT calculation in four basis set (cc-pVDZ, aug-cc-pvDZ, cc-pVTZ, aug-cc-pVTZ). Values in parentheses are atomic charges with hydrogens summed into heavy atoms.

studies.[10] Another experimental evidence of spin localization is the formation of $C_6H_5SSC_6H_5$ as the dominant combination product.[10]

b. Vertical and Adiabatic A $^2B_2$ ← X $^2B_1$ Excitation Energies and Assignment of Higher Electronic States. The computed vertical, adiabatic, and 0−0 excitation energies for the X $^2B_1$ → A $^2B_2$ transition are given in Table 2. All the employed methods give rather similar theoretical estimates of the excitation energy. The results do not depend strongly on the quality of the basis set used in the calculations. The computed MRCI+Q, CASPT2, DFT, and TDDFT adiabatic and vertical excitation energies do not differ by more than 0.12 eV than the reported experimental value of 0.323 eV.[19−21] Bearing in mind that the accuracy of the employed computational methods is probably not better than 0.1 eV, the agreement between theory and experiment can be considered as good. The best agreement between theory and experiment is found for the MRCI+Q/aug-cc-pVTZ method with the assumption that the experimentally determined value corresponds to adiabatic excitation energy. Excellent agreement with experiment for the previously reported[19,20] CASPT2 excitation energy (0.332 eV), which was computed in smaller active space, is probably somewhat fortuitous. The experimental excitation energy was reported by Kim and co-workers, who investigated the photolysis of thiophenol (C_6H_5SH or C_6H_5SD) at 243 nm using the H^+ (D^+) velocity map imaging technique.[19−21] Two distinct anisotropic rings observed in the H^+ (D^+) images were identified to correspond to production of two lowest electronic states of the C_6H_5S radical upon H (D) detachment. A value of 0.323 ± 0.024 eV (2600 ± 200 cm^{-1}) determined from the difference in threshold translational energy between these two channels was attributed to the energy difference between the A $^2B_2$ and X $^2B_1$ states of C_6H_5S. Is it possible that the experimental value of 0.323 eV corresponds to the energy separation between the X $^2B_1$ and A $^2B_2$ states of the thiophenoxyl radical *at the frozen equilibrium geometry of* C_6H_5SD? If this interpretation is correct, the somewhat larger value obtained in our calculations and excellent agreement between MRCI+Q, CASPT2, DFT, and TDDFT can be easily understood. We hope that our future study of the A $^2B_2$ state of the thiophenoxyl radical using cavity ringdown absorption spectroscopy will help to shed more light on this issue.

In our recent studies[26,47] of the first excited state of the phenoxyl radical, we reported theoretical and experimental energy separation between the two lowest electronic states of C_6H_5O. Unfortunately, the previous experimental values[27,28] of the separation could not be uniquely assigned as the vertical or adiabatic excitations due to discrepancies in our computed data. We try to compensate for this omission in the present work by comparing the experimental values for the phenoxyl radical with accurate MRCI+Q theoretical data. As can be seen from data shown in Table 3, the MRCI+Q vertical excitation energies lie between the previously reported CASPT2 and B3LYP results and the MRCI+Q adiabatic excitation energies are almost identical to those computed with B3LYP.[26] The presented MRCI+Q results suggest that the previously published experimental excitation energies should be interpreted as vertical excitations. This is also consistent with the experimental adiabatic separation between these two states that was found by us to be 0.952 eV.[47]

No definitive assignment of higher lying electronic states of the thiophenoxyl radical is available. Since the only published theoretical study of excited states was performed using a low-level quantum chemical method (configuration interaction with

TABLE 2: Total Energies, Vertical Excitation Energies, and Adiabatic Excitation Energies for the X $^2B_1$ and A $^2B_2$ Electronic States of the Thiophenoxyl Radical Computed Using the CASSCF, CASPT2, MRCI+Q, and B3LYP Methods[d]

	total energies			A $^2B_2$ ← X $^2B_1$ excitation energies		
basis set	X $^2B_1$	A $^2B_2$ (vertical)	A $^2B_2$ (adiabatic)	vertical[a]	adiabatic	ΔE_H^{0-0}[b]
			CASSCF			
cc-pVDZ	−627.726063	−627.713627	−627.714759	0.338	0.308	0.303
aug-cc-pVDZ	−627.733670	−627.721080	−627.722244	0.343	0.311	0.310
cc-pVTZ	−627.795487	−627.783484	−627.784651	0.327	0.295	0.292
aug-cc-pVTZ	−627.797276	−627.785374	−627.786538	0.324	0.292	0.290
			CASPT2			
cc-pVDZ	−628.552552	−628.537445	−628.538731	0.411	0.376	0.371
aug-cc-pVDZ	−628.598634	−628.582527	−628.583904	0.438	0.401	0.400
cc-pVTZ	−628.824789	−628.809950	−628.811244	0.404	0.369	0.366
aug-cc-pVTZ	−628.844566	−628.829445	−628.830767	0.412	0.376	0.374
			MRCI+Q			
cc-pVDZ	−628.580901	−628.567184	−628.568948	0.373	0.325	0.320
aug-cc-pVDZ	−628.619835	−628.605467	−628.607377	0.391	0.339	0.338
cc-pVTZ	−628.830279	−628.816726	−628.818590	0.369	0.318	0.315
aug-cc-pVTZ	−628.846297	−628.832556	−628.834465	0.374	0.322	0.320
			B3LYP			
cc-pVDZ	−629.842725	−629.826715	−629.827936	0.436 (0.403)	0.403	0.398
aug-cc-pVDZ	−629.856466	−629.840607	−629.841813	0.432 (0.412)	0.399	0.398
cc-pVTZ	−629.924651	−629.909312	−629.910475	0.417 (0.428)	0.386	0.383
aug-cc-pVTZ	−629.927282	−629.911999	−629.913156	0.416 (0.433)	0.384	0.382
exptl				0.323 ±0.010[c]		

[a] Values in parentheses have been calculated using the TDDFT method. [b] Isotope substitution of hydrogen by deuterium does not alter these values. [c] References 19, 20, and 21. [d] All CASSCF, CASPT2, and MRCI+Q calculations use the same ($0a_1$, $2a_2$, $5b_1$, $1b_2$) active space described in detail in the text. ΔE_H^{0-0} denotes the 0−0 excitation energy for C_6H_5S. Total energies are given in hartree and excitation energies in eV.

TABLE 3: Total Energies, Vertical Excitation Energies, and Adiabatic Excitation Energies for the X $^2B_1$ and A $^2B_2$ Electronic States of the Phenoxyl Radical Computed Using the MRCI+Q Method at the Optimized CASPT2 Geometries[c]

	total energies			A $^2B_2$ ← X $^2B_1$ excitation energies			
basis set	X $^2B_1$	A $^2B_2$ (vertical)	A $^2B_2$ (adiabatic)	vertical[a]	adiabatic	ΔE_H^{0-0}	ΔE_D^{0-0}
			MRCI+Q				
cc-pVDZ	−305.945344	−305.903375	−305.912976	1.142	0.881	0.880	0.878
aug-cc-pVDZ	−305.990382	−305.947200	−305.957020	1.175	0.908	0.904	0.903
cc-pVTZ	−306.210359	−306.167617	−306.177899	1.163	0.883	0.880	0.878
aug-cc-pVTZ	−306.228308	−306.185093	−306.195206	1.176	0.901	0.898	0.896
exptl						1.06,[a] 1.10[b]	

[a] Reference 27, in the gas phase. [b] Reference 28, in argon matrix. [c] All calculations use the same ($0a_1$, $2a_2$, $5b_1$, $1b_2$) active space described in detail in ref 26. ΔE_H^{0-0} denotes the 0−0 excitation energy for C_6H_5O, and ΔE_D^{0-0} for C_6D_5O. Total energies are given in hartree and excitation energies in eV.

single excitations only), we use this opportunity to report here the low-lying doublet states of the thiophenoxyl radical. The calculated TDDFT and MS CASPT2 excitation energies are tabulated in Table 4 for all electronic states under 4.5 eV (275 nm). For the TDDFT method, the corresponding transition oscillator strengths are also given. The quality of the basis set does not have a substantial impact on the calculated excitation energies (except for the $^2A_1$ state at the CASPT2 level). A relatively large number of electronic states are located in the studied spectral region. It is not a difficult task to explain the reported experimental absorption and fluorescence data in terms of the calculated electronic spectrum. The fluorescence excitation signals observed[17] by Shibuya et al. in the gas phase between 2.38 and 2.58 eV correspond to the $^2A_2$ state located by us at 2.44 (TDDFT) and 2.34 eV (CASPT2). This finding confirms the suggested experimental assignment for this state. The 0−0 band was assigned by Shibuya et al.[17] at 2.40 eV and earlier by Okuyama et al.[16] at 2.51 eV. The absorption attributed to the $^2A_2$ state is weak; the calculated oscillator strength is only 0.002. This state is probably also responsible for the weak shoulder band observed[11] in absorption spectrum in solution at 2.44 eV. The main broad signal in the absorption spectrum in solution has a maximum at 2.70 eV together with intensive sideband at 2.57 eV.[10] A similar broad signal is also observed in the emission spectrum.[13,14] The position of the maximum in the absorption spectrum depends quite strongly on the solvent: 2.70 eV in water,[10,11] 2.79 eV in decalin,[1] 2.91 eV in 3-methylpentane,[13] and 2.92 eV in ethanol.[2] It is plausible to assign this band to the calculated $^2B_1$ state, which is located in our calculations at 3.00 (TDDFT) and 2.66 eV (CASPT2), and the observed sideband to progression associated with some ∼1050 cm^{-1} vibrational mode. It is possible that the 0−0 band is weak and both the observed bands correspond to progressions. The calculated oscillator strength for the $^2B_1$ state is large (0.059) and explains well the observed absorption spectrum. The most intensive peak in the absorption spectrum is located at 4.20 eV in aqueous solution[10,11] and at 4.17 eV in cyclohexane and ethanol.[2] It is clear that the state responsible for this peak is

TABLE 4: Vertical Excitation Energies (in eV) for the Lowest Doublet Excited States of the Thiophenoxyl Radical Computed Using the B3LYP and Multistate (MS) CASPT2 Method[h]

	TDDFT				MS CASPT2				
	cc-pVDZ	aug-cc-pVDZ	cc-pVTZ	aug-cc-pVTZ	cc-pVDZ	aug-cc-pVDZ	cc-pVTZ	aug-cc-pVTZ	Exp.
X^2B_1	−629.842725	−629.856466	−629.924651	−629.927282	−628.549286	−628.594568	−628.820821	−628.840438	
$^2B_2$	0.403 (0.000)	0.412 (0.000)	0.428 (0.000)	0.433 (0.000)	0.454	0.487	0.451	0.461	0.323[a]
$^2A_2$	2.430 (0.003)	2.383 (0.002)	2.457 (0.003)	2.443 (0.002)	2.547	2.357	2.412	2.344	2.40[b], 2.51[c]
$^2B_1$	3.001 (0.054)	2.952 (0.061)	3.013 (0.057)	2.999 (0.059)	2.718	2.633	2.693	2.664	2.70[d], 2.79[e], 2.91[f], 2.92[g]
$^2A_1$	3.947 (0.003)	3.908 (0.002)	3.949 (0.003)	3.944 (0.002)	4.820	4.689	4.751	4.265	
$^2B_1$	4.186 (0.049)	4.133 (0.061)	4.223 (0.058)	4.197 (0.066)	4.729	4.604	4.746	4.662	4.20[d], 4.17[g]
$^2B_2$	4.458 (0.000)	4.379 (0.000)	4.438 (0.000)	4.393 (0.000)	4.265	4.208	4.257	4.225	
$^2A_2$	4.536 (0.011)	4.424 (0.008)	4.514 (0.010)	4.459 (0.008)	5.262	5.063	5.196	5.084	

[a] References 19, 20, and 21. Photoelecton spectroscopy in the gas phase. [b] Reference 13. Fluorescence in the gas phase. [c] Reference 12. Fluorescence in the gas phase. [d] References 11 and 14. Time-resolved absorption spectroscopy in aqueous solution. [e] Reference 1. Time-resolved absorption spectroscopy in liquid decalin. [f] Reference 17. Absorption spectrum in 3-methylpentane glass. [g] Reference 2. Absorption spectrum in cyclohexane and EtOH. [h] The lowest excited state in each symmetry is given. Values in parentheses are oscillator strengths.

TABLE 5: Harmonic Vibrational Frequencies for the X $^2B_1$ and A $^2B_2$ Electronic State of C_6H_5S Computed Using the B3LYP Method[c]

		X $^2B_1$					A $^2B_2$			
symmetry	mode	exptl	cc-pVDZ	aug-cc-pVDZ	cc-pVTZ	aug-cc-pVTZ	cc-pVDZ	aug-cc-pVDZ	cc-pVTZ	aug-cc-pVTZ
A_1	υ_1		3117	3115	3105	3104	3111	3110	3099	3099
	υ_2		3104	3103	3093	3092	3097	3096	3086	3086
	υ_3		3084	3085	3073	3073	3079	3081	3069	3069
	υ_4	1551[a]	1559	1549	1552	1549	1586	1574	1575	1571
	υ_5		1431	1423	1444	1441	1451	1442	1463	1460
	υ_6	1180[a], 1165[b]	1153	1155	1166	1164	1160	1162	1173	1171
	υ_7	1073[a]	1049	1044	1051	1051	1068	1063	1068	1066
	υ_8		1008	1004	1012	1010	1017	1013	1018	1017
	υ_9	991[a]	976	968	980	979	976	971	983	983
	υ_{10}	724[a]	708	706	711	710	683	683	687	686
	υ_{11}	436[a], 430[b]	415	413	415	415	397	396	399	398
A_2	υ_{12}		967	958	971	974	949	944	951	957
	υ_{13}		827	816	828	828	820	811	823	825
	υ_{14}		376	375	376	373	410	409	411	409
B_1	υ_{15}		987	975	986	986	972	965	972	976
	υ_{16}		919	910	923	924	880	871	884	887
	υ_{17}		749	744	753	752	721	716	726	725
	υ_{18}		669	664	671	668	685	684	688	684
	υ_{19}		453	452	454	451	464	465	466	464
	υ_{20}		157	156	156	156	175	174	175	174
B_2	υ_{21}		3113	3113	3102	3101	3101	3100	3090	3089
	υ_{22}		3093	3093	3083	3082	3085	3086	3075	3075
	υ_{23}		1539	1529	1534	1531	1566	1557	1558	1555
	υ_{24}		1414	1404	1422	1420	1414	1403	1421	1419
	υ_{25}		1310	1304	1306	1305	1308	1305	1316	1314
	υ_{26}		1262	1260	1265	1263	1265	1262	1255	1253
	υ_{27}		1134	1136	1147	1144	1137	1138	1149	1147
	υ_{28}		1059	1059	1065	1064	1062	1061	1066	1064
	υ_{29}	610[b]	600	597	604	603	606	605	612	610
	υ_{30}		289	288	289	288	238	238	237	237

[a] Reference 11. Resonance Raman in solution. [b] Reference 13. Fluorescence in the gas phase. [c] All values are given in cm^{-1}.

$^2B_1$ with the calculated excitation energy of 4.20 (TDDFT) and 4.66 eV (CASPT2), and the largest oscillator strength (0.066) among all theoretically determined electronic states. There exists a large discrepancy between the TDDFT and CASPT2 methods for some higher lying states (the first $^2A_1$ and second $^2A_2$ states). Usually such large discrepancy is attributed to inaccuracies within the TDDFT scheme, but here it also can be caused by deficiencies in the choice of the active space or poor convergence of the perturbation series. (Note the large deviation of the $^2A_1 \leftarrow X\ ^2B_1$ CASPT2 transition energy computed with various basis sets.) The lowest quartet state of the thiophenoxyl radical ($^4B_1$) is found at 4.35 eV in our B3LYP/cc-pVDZ calculations. Clearly, higher spin states are not going to influence the observed absorption spectrum of C_6H_5S in the studied spectral region. Our calculations cannot account directly for the red emission observed[13,14] in the photolysis of C_6H_5SH and $C_6H_5SSC_6H_5$ in 3-methylpentane and EPA glasses. (The emission maximum is located at 1.83 eV in 3MP and at 1.92 eV in EPA; well-structured vibrational progression of approximately 1350 cm^{-1} is also observed.) The only electronic state located in this region is $^2B_1$, but the observed emission maxima differ by 0.5−0.6 eV to match this state. It is rather unlikely that there exists another electronic state with such energy, especially given that the positions of the next two observed states, $^2A_2$ with $^2B_1$,

TABLE 6: Harmonic Vibrational Frequencies for the X $^2B_1$ and A $^2B_2$ Electronic State of C_6D_5S Computed Using the B3LYP Method[a]

		X $^2B_1$				A $^2B_2$			
symmetry	mode	cc-pVDZ	aug-cc-pVDZ	cc-pVTZ	aug-cc-pVTZ	cc-pVDZ	aug-cc-pVDZ	cc-pVTZ	aug-cc-pVTZ
A_1	ν_1	2311	2310	2301	2301	2308	2307	2298	2298
	ν_2	2296	2295	2287	2286	2289	2289	2281	2280
	ν_3	2273	2273	2266	2266	2268	2270	2262	2262
	ν_4	1521	1510	1508	1505	1550	1538	1536	1532
	ν_5	1296	1286	1297	1295	1319	1309	1319	1316
	ν_6	1023	1016	1026	1026	1026	1020	1027	1026
	ν_7	935	928	940	939	936	931	942	941
	ν_8	843	844	853	851	849	850	860	858
	ν_9	807	808	816	815	813	813	821	820
	ν_{10}	670	668	673	673	650	650	655	654
	ν_{11}	407	405	408	407	390	389	391	391
A_2	ν_{12}	786	781	789	793	770	769	772	779
	ν_{13}	643	634	644	644	639	631	640	642
	ν_{14}	327	325	327	325	357	355	358	356
B_1	ν_{15}	826	821	829	827	808	809	810	813
	ν_{16}	756	751	761	761	725	722	731	732
	ν_{17}	630	624	632	631	609	604	611	610
	ν_{18}	520	514	521	520	535	530	536	535
	ν_{19}	400	398	400	398	408	407	409	407
	ν_{20}	148	146	147	146	164	163	164	163
B_2	ν_{21}	2305	2304	2295	2295	2297	2296	2287	2287
	ν_{22}	2283	2283	2275	2275	2276	2277	2268	2269
	ν_{23}	1495	1485	1484	1481	1530	1520	1517	1514
	ν_{24}	1322	1314	1310	1308	1314	1304	1302	1300
	ν_{25}	1272	1263	1258	1256	1266	1257	1249	1247
	ν_{26}	998	996	1017	1016	1000	998	1018	1016
	ν_{27}	824	824	834	832	822	822	832	830
	ν_{28}	798	801	810	809	806	809	817	815
	ν_{29}	575	574	580	579	581	580	586	585
	ν_{30}	275	273	274	274	226	227	226	226

[a] All values are given in cm^{-1}.

agree well with our calculations. We can see two potential explanations for this phenomenon.

(1) The emission corresponds rather to the B $^2A_2 \rightarrow$ A $^2B_2$ transition than the B $^2A_2 \rightarrow$ X $^2B_1$ transition. The calculated energy separation between the B $^2A_2$ and A $^2B_2$ states is 2.01 eV (TDDFT/aug-cc-pVTZ), which matches the experimental emission spectrum more closely than the energy separation between B $^2A_2$ and X $^2B_1$ (2.44 eV). Even better agreement is observed for the associated excitation spectrum (see Figure 2 of ref 14), which has a maximum located at 2.11 eV. This value almost perfectly agrees with the experimentally determined separation between the B $^2A_2$ and A $^2B_2$ states (2.08 eV).

(2)The equilibrium geometry of the B $^2A_2$ state computed with DFT is not planar. There exists a close structural similarity with the equilibrium geometry of the phenoxyl radical in the $^2A''$ state. (For details, see Figure 2 of ref 48.) It is clear that geometry relaxation leads to smaller energy separation between the B $^2A_2$ state and the two lower states. However, the energy of the B $^2A_2$ state is lowered only by 0.002 eV (B3LYP/cc-pVDZ) upon the relaxation. At the same time, the energy of the two lower states computed at the optimized geometry of the B $^2A_2$ state is elevated by 0.36 (X $^2B_1$) and 0.40 eV (A $^2B_2$). The zero-point energy corrections (cc-pVDZ, unscaled) to all three studied states are comparable (2.46, 2.46, and 2.37 eV for X $^2B_1$, A $^2B_2$, and B $^2A_2$, respectively). The experimental separation between the maxima of emission and absorption signals is 0.28 eV in 3MP and 0.19 eV in EPA. It is rather unlikely that this mechanism could account for the discrepancy of 0.5−0.6 eV for the B $^2A_2 \rightarrow$ X $^2B_1$ transition mentioned above.

Note that none of these hypotheses fully explains the unusually long lifetime of the observed red emission. Jinguji et al.[14] argue that the long emission lifetime is a consequence of the strongly forbidden character of the corresponding excitation. The computed TDDFT oscillator strengths for the B $^2A_2 \rightarrow$ A $^2B_2$ and B $^2A_2 \rightarrow$ X $^2B_1$ transitions are indeed small: 0.002 and 0.000, respectively.

There is no experimental evidence for other electronic states of the thiophenoxyl radical with excitation energies smaller than 4.5 eV.

c. Harmonic Vibrational Frequencies. Harmonic vibrational frequencies for the X $^2B_1$ and A $^2B_2$ states of C_6H_5S are given in Table 5. Analogous data for the isotope-substituted species (C_6D_5S) are given in Table 6. The presented (scaled) values are computed with B3LYP using a set of four basis sets. The scaling factors (0.971 for cc-pVDZ and aug-cc-pVDZ and 0.970 for cc-pVTZ and aug-cc-pVTZ) have been determined from separate DFT calculations for thiophenol (C_6H_5SH), for which experimental fundamental frequencies are available.[49] The frequencies computed with various basis sets are rather similar; the largest deviation observed upon basis set change is 21 cm^{-1} for ν_{26} of C_6D_5S (X $^2B_1$) and ν_5 of C_6H_5S (A $^2B_2$). As discussed in the previous study of the phenoxyl radical,[26] the smallest mean absolute deviation from experiment (approximately 25 cm^{-1}) can be expected for the cc-pVTZ basis set. Therefore, for the following discussion, the cc-pVTZ harmonic vibrational frequencies are used. A graphical description of some of the full-symmetric modes can be found in ref 10. Information for the remaining vibrational modes will be made available from the authors upon request.

The change in harmonic vibrational frequencies upon the X $^2B_1 \rightarrow$ A $^2B_2$ excitation is small. The difference between the zero-point energies (ZPE) of both states is only 26 cm^{-1} for C_6H_5S and 37 cm^{-1} for C_6D_5S. On average, each vibrational level is displaced by 15 cm^{-1} for C_6H_5S and 13 cm^{-1} for C_6D_5S. The largest displacement is observed for the in-plane CS bending (ν_{30}): -51 cm^{-1} for C_6H_5S and -48 cm^{-1} for C_6D_5S. The change in other vibrational modes involving the sulfur atom—the out-of-plane CS bending (ν_{20}) and the CS stretch (ν_7)—is noticeably smaller. This situation is in contrast with that reported[26] for the phenoxyl radical, where the corresponding vibrational modes (ν_6, ν_{30}, and ν_{20}) were displaced by 167, 73, and 38 cm^{-1} (C_6H_5O) and 217, 65, and 37 cm^{-1} (C_6D_5O), respectively.

The computed harmonic vibrational frequencies of the ground state correspond well to the fundamental modes detected in the resonance Raman spectrum in solution (436, 724, 991, 1073, 1180, and 1551 cm^{-1})[10] and in the gas-phase fluorescence spectrum (430, 610, and 1165 cm^{-1}).[17] These modes can be easily assigned to ν_{11}, ν_{10}, ν_9, ν_7, ν_6, and ν_4 (solution spectrum) and to ν_{11}, ν_{29}, and ν_6 (gas-phase spectrum). (For more detailed discussion, see ref 10.) The computed ground-state frequencies are in satisfactory agreement with other theoretical studies.[10,22,25] Similar agreement is found for the X $^2B_1$ and A $^2B_2$ frequencies reported by Song et al.,[23] if one scales these frequencies by an appropriate factor. While no large discrepancies are found with the previous theoretical data, the present study probably can be considered as giving the most accurate set of harmonic vibrational frequencies for both electronic states of the thiophenoxyl radical owing to the most complete character of employed basis sets.

The presented analysis confirms the observation made previously on the basis of optimized geometrical parameters about structural similarity between both electronic states of the thiophenoxyl radical. The computed force fields are also similar giving an almost identical set of harmonic vibrational frequencies for both electronic states: X $^2B_1$ and A $^2B_2$.

Conclusion

High-level ab initio techniques are employed to study the equilibrium geometry, excitation energies, and harmonic vibrational frequencies for the first excited electronic state (A $^2B_2$) of the thiophenoxyl radical. The calculated properties are compared to analogous data for the ground state. The wave functions of both studied electronic states are well represented with single Slater determinants. The A $^2B_2 \leftarrow$ X $^2B_1$ excitation can be concisely described as a transfer of a single electron between two atomic-like p orbitals localized on sulfur. The calculated excitation energies for the A $^2B_2 \leftarrow$ X $^2B_1$ transition correspond well to experimental data. The change in molecular equilibrium geometry and harmonic vibrational frequencies is rather small upon the excitation. The presented results show that the A $^2B_2 \leftarrow$ X $^2B_1$ excitation in C_6H_5S has a quite different characteristic than the analogous transition in the phenoxyl radical (C_6H_5O), where the singly occupied orbital in the X $^2B_1$ state is largely delocalized over oxygen and the aromatic ring. The delocalization causes energetic stabilization of the X $^2B_1$ state of C_6H_5O and results in approximately double character of the CO bond. This effect is missing in C_6H_5S owing to a much larger distance between sulfur and carbon that does not permit large effective overlap of π densities on both atoms. Consequently, both studied electronic states of the thiophenoxyl radical (A $^2B_2$ and X $^2B_1$) show close energetic and structural similarity.

In addition, a computational study of other low-lying (<4.5 eV) electronic states of the thiophenoxyl radical is presented. The calculated TDDFT and CASPT2 excitation energies correspond well to the available experimental absorption and emission data. A reliable assignment of excited states of the thiophenoxyl radical is given in Table 4. The lowest quartet state of C_6H_5S is found at 4.35 eV (B3LYP/cc-pVDZ).

Acknowledgment. We thank Prof. Soji Tsuchiya for help and the National Center for High-Performance Computing for computer time. The National Science Council of Taiwan is acknowledged for financial support (grants NSC96-2113-M009-022 and NSC96-2113-M009-025). This research has also been supported by Institute of Nuclear Energy Research, Atomic Energy Council, Taiwan, under Contract No. 970147 L, and by the Ministry of Education (MOE-ATU project).

References and Notes

(1) Scott, T. W.; Liu, S. N. *J. Phys. Chem.* **1989**, *93*, 1393.
(2) Thyrion, F. C. *J. Phys. Chem.* **1973**, *77*, 1478.
(3) Gaspari, G.; Granzow, A. *J. Phys. Chem.* **1970**, *74*, 836.
(4) Ito, O.; Matsuda, M. *J. Am. Chem. Soc.* **1983**, *105*, 1937.
(5) Ito, O.; Matsuda, M. *J. Am. Chem. Soc.* **1979**, *101*, 1815.
(6) Ito, O.; Matsuda, M. *J. Am. Chem. Soc.* **1979**, *101*, 5732.
(7) Burkey, T. J.; Griller, D. *J. Am. Chem. Soc.* **1985**, *107*, 246.
(8) Hermann, R.; Dey, G. R.; Naumov, S.; Brede, O. *Phys. Chem. Chem. Phys.* **2000**, *2*, 1213.
(9) Armstrong, D. A.; Sun, Q.; Schuler, R. H. *J. Phys. Chem.* **1996**, *100*, 9892.
(10) Tripathi, G. N. R.; Sun, Q.; Armstrong, D. A.; Chipman, D. M.; Schuler, R. H. *J. Phys. Chem.* **1992**, *96*, 5344.
(11) Bonifačić, M.; Weiss, J.; Chaudhri, S. A.; Asmus, K.-D. *J. Phys. Chem.* **1985**, *89*, 3910.
(12) Feher, F.; Gladden, T.; Kurz, D. *Z. Naturforsch.* **1970**, *25b*, 1215.
(13) Russell, P. G. *J. Phys. Chem.* **1975**, *79*, 1353.
(14) Jinguji, M.; Imamura, T.; Obi, K.; Tanaka, I. *Chem. Phys. Lett.* **1984**, *109*, 31.
(15) Porter, G.; Wright, F. J. *Trans. Faraday Soc.* **1955**, *51*, 1469.
(16) Okuyama, M.; Takakura, T.; Kamada, H. *J. Spectrosc. Soc. Jpn.* **1977**, *26*, 164.
(17) Shibuya, K.; Nemoto, M.; Yanagibori, A.; Fukushima, M.; Obi, K. *Chem. Phys.* **1988**, *121*, 237.
(18) Norrish, R. G. W.; Zeelenberg, A. P. *Proc. R. Soc. London, Ser. A* **1967**, *240*, 293.
(19) Lim, J. S.; Lim, I. S.; Lee, K. S.; Ahn, D. S.; Lee, Y. S.; Kim, S. K. *Angew. Chem., Int. Ed.* **2006**, *45*, 6290.
(20) Lim, I. S.; Lim, J. S.; Lee, Y. S.; Kim, S. K. *J. Chem. Phys.* **2007**, *126*, 034306.
(21) Lim, J. S.; Lee, Y. S.; Kim, S. K. *Angew. Chem., Int. Ed.* **2008**, *47*, 1853.
(22) Kamisuki, T.; Hirose, C. *J. Mol. Struct. (THEOCHEM)* **2000**, *531*, 51.
(23) Remacle, F.; Kryachko, E. S. *J. Mol. Struct.* **2004**, *708*, 165.
(24) Song, L.; Bu, Y; Li, P. *Int. J. Quantum Chem.* **2005**, *105*, 186.
(25) Xu, W.; Gao, A. *J. Phys Chem. A* **2006**, *110*, 997.
(26) Cheng, C.-W.; Lee, Y.-P.; Witek, H. A. *J. Phys. Chem. A* **2008**, *112*, 2648.
(27) Radziszewski, J. G.; Gil, M.; Gorski, A.; Spanget-Larsen, J.; Waluk, J.; Mróz, B. J. *J. Chem. Phys.* **2001**, *115*, 9733.
(28) Gunion, R. F.; Gilles, M. K.; Polak, M. L.; Lineberger, W. C. *Int. J. Mass Spectrom. Ion Processes* **1992**, *117*, 601.
(29) Foster, S. C.; Miller, T. A. *J. Phys. Chem.* **1989**, *93*, 5986.
(30) Werner, H.-J. *Mol. Phys.* **1996**, *89*, 645.
(31) Celani, P.; Werner, H.-J. *J. Chem. Phys.* **2000**, *112*, 5546.
(32) Casida, M. E.; Jamorski, C.; Casida, K. C.; Salahub, D. R. *J. Phys. Chem.* **1998**, *108*, 4439.
(33) Finley, J.; Malmqvist, P.-Å; Roos, B. O.; Serrano-Andrés, L. *Chem. Phys. Lett.* **1998**, *288*, 299.
(34) Dunning, T. H., Jr *J. Chem. Phys.* **1989**, *90*, 1007.
(35) Kendall, R. A.; Dunning, T. H, Jr.; Harrison, R. J. *J. Chem. Phys.* **1992**, *96*, 6769.
(36) Werner, H.-J.; Knowles, P. J.; Amos, R. D. et al., *MOLPRO*, a package of ab initio programs, version 2006.1.
(37) Frisch, M. J.; Trucks, G. W.; Schlegel, H. B. et al. *Gaussian 03*, Revision A.1; Gaussian Inc.: Pittsburgh, PA,2003.
(38) Becke, A. D. *J. Chem. Phys.* **1993**, *98*, 5648.
(39) Lee, C.; Yang, W.; Parr, R. G. *Phys. Rev. B* **1988**, *37*, 785.
(40) Kohn, W.; Sham, L. J. *Phys. Rev.* **1965**, *140*, A1133.

(41) NIST Computational Chemistry Comparison and Benchmark Database, NIST Standard Reference Database Number 101, Release 12, Aug 2005, Russell D. Johnson III, Ed. http://srdata.nist.gov/cccbdb.
(42) Hagen, K.; Hedberg, K. *J. Chem. Phys.* **1973**, *59*, 158.
(43) Chipman, D. M.; Liu, R.; Zhou, X.; Pulay, P. *J. Chem. Phys.* **1994**, *100*, 5023.
(44) Johansson, K. I.; Oldeberg, H.; Selen, H. *Ark. Fys.* **1967**, *33*, 313.
(45) Allen, F. H.; Kennard, O.; Watson, D. G.; Brammer, L.; Orpen, A. G.; Taylor, R. *J. Chem. Soc., Perkin Trans.* **1987**, *2*, S1.
(46) Visscher, L.; Dyall, K. G. *At. Data Nucl. Data Tables* **1997**, *67*, 207.
(47) Cheng, C.-W.; Witek, H. A.; Lee, Y.-P. *J. Chem. Phys.* In press.
(48) Liu, R.; Morokuma, K.; Mebel, A. M.; Lin, M. C. *J. Phys. Chem.* **1996**, *100*, 9314.
(49) Scott, D. W.; McCullough, J. P.; Hubbard, W. N.; Messerly, J. F.; Hossenlopp, I. A.; Waddington, G. *J. Am. Chem. Soc.* **1956**, *78*, 5463.

JP805045S